

# ANALYTICAL $C^3$ CONTINUOUS TOOL PATH SMOOTHING ALGORITHM FOR ROBOTIC MACHINING CONSIDERING THE REDUNDANT ANGLE

Qin Hu,\* Runqi Yang,\* Xu Zhang,\* and Liang Huang\*

## Abstract

The corner smoothing method is commonly used to smooth linear tool paths of robotic machining, and the robot pose optimisation method is usually adopted to improve robot stiffness. However, the robot pose is optimised by adjusting the redundant angle, which does not affect the tool pose and has not been considered in the process of tool path smoothing. The discontinuous redundant angle affects the continuity of the robotic axis motion, which would result in breakage. This study proposes an innovative  $C^3$  continuous robotic tool path smoothing method with shape-preserving, redundant angle, and accurate real-time interpolations. First, to ensure accurate real-time interpolation, only the tooltip position corner is smoothed by the  $C^3$  continuous Pythagorean-hodograph spline with the error tolerance constraint. Second, the tool orientation and redundant angle are smoothed by the  $C^3$  continuous B-spline, which has fewer control points and more efficient interpolation. Third, to guarantee the synchronisation of the three smoothed tool paths, a transitive synchronisation strategy is proposed. The simulations and experiments verified that the proposed method could obtain jerk continuous axis motion with shape-preserving interpolation. Comparative experiments showed that the proposed method could significantly reduce the tracking error of each axis.

## Key Words

Robotic machining, tool path smoothing,  $C^3$  continuity, redundant angle, synchronisation

## 1. Introduction

Industrial robots have lower cost, larger workspace, and stronger generality than computer numerical control

machine tools [1]. Industrial robots are suitable for the flexible processing of multi-specification parts in multiple scenarios. When equipped with a mobile platform and multirobot collaboration mode, industrial robots can further increase the workspace and improve processing flexibility and efficiency [2], [3]. However, the machining path command is usually a sequence of discrete tool cutting locations, and the tool experiences frequent acceleration and deceleration during its movement along the discrete tool cutting locations, which restricts the robotic machining efficiency and stability [4], [5]. High-order continuous path smoothing is important to improve the efficiency and accuracy of the robotic machining process [6], [7].

The tool path smoothing of robots is initially applied in the joint space and improves the efficiency of the robot in completing tasks, such as handling. The smoothing method in the joint space directly smooths the discrete joint commands. The advantage is that the planned joint paths can be directly used to drive robot joints without further kinematic transformations [8]–[10]. However, because of the strong nonlinear kinematics of the robot, this method encounters difficulties in constraining the trajectory smoothing error at the end of the tool and is unsuitable for precise contour motion scenarios.

In the task space, the tool path is represented by the tooltip position and tool orientation in the workpiece coordinate system (WCS). To ensure the smooth movement of each joint axis of the robot, both the tool position and tool orientation need to be smooth [11]. In addition, the position and posture after smoothing need to be synchronised to ensure high-order continuity of joint displacement [12], [13]. The mainstream methods include global smoothing [14], [15] and local corner smoothing [16]. Direct corner smoothing of the tool path makes it easy to constrain the actual deviation between the smoothed and reference paths. Sun *et al.* [17] adopted the FIR filter interpolation method to generate the smooth tool pose for the 6R robot manipulator, the tool pose deviations are all constrained by special designing the overlapping time at the corners. Peng *et al.* [18] proposed a decoupled

\* School of Automation, Wuhan University of Technology, Wuhan, Hubei, China; e-mail: qinhu@whut.edu.cn; 905246503@qq.com; 1394216332@qq.com; 35644519@qq.com  
Corresponding author: Qin Hu

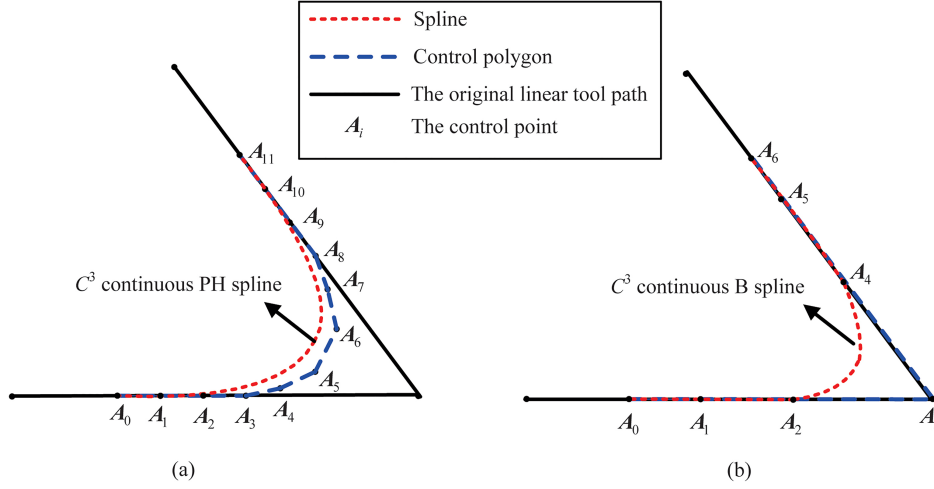


Figure 1.  $C^3$  continuous splines of (a) PH spline and (b) B-spline.

local smoothing method for industrial robots and the orientation error is constrained analytically. The path deviation of robot milling directly affects the machining quality. Therefore, the robot milling tool path smoothing method needs to be investigated under the error tolerance constraints in the task space.

The tool path smoothing method of the robot end usually uses microsplines instead of tooltip position path corners and tool orientation corners. To ensure jerk continuous axis motion, the tooltip position and tool orientation after smoothing need to be synchronised to ensure high-order continuity of tooltip displacement. The commonly used microsplines include B-splines [19]–[21], Non-Uniform Rational B-Splines (NURBS) splines [22], [23], Bézier splines [24], [25], and Pythagorean-hodograph (PH) splines [9], [26], [27]. B-spline is a commonly used parameter curve that can be locally modified. Huang *et al.* [21] adopted B-splines smoothing linear segments, and proposed the smoothing method as not only smoothing the corner in the convex side, but back and forth between the convex and concave sides to decrease the maximum curvature. NURBS splines can not only be locally modified, but also precisely control the shape of curves to meet specific geometric requirements. Liu *et al.* [22] proposed a high-precision interpolation system by segmenting global NURBS curve into a collection of Bézier splines to meet the chord error constraint. The form of Bézier spline curve is relatively simpler compared to the B-spline and NURBS spline, so it is widely used in path planning. Sencer *et al.* [25] proposed a geometric corner smoothing algorithm based on quintic Bézier spline and obtained the optimal curvature geometry. The PH spline form is the same as Bézier spline, but more complex than the Bézier spline with the same parameter continuous. The biggest advantage of PH spline over the above spline is that the arc length can be analytically calculated.

The B-spline control point has strong flexibility in terms of setting, but the disadvantage is that the arc length cannot be analytically calculated. The calculation of the path length of the smoothed tooltip position can only be done by numerical approximation methods,

which have a large computational load and low accuracy [28]. In addition, Taylor expansion is commonly used to solve spline parameters based on arc length during the interpolation process, which may result in truncation errors. The truncation errors could cause axis acceleration and jerk jumps at both ends of the spline, even exceeding the set value. The NURBS and Bézier splines have the same problem as the B-spline. However, the length of the PH spline is a polynomial of the spline parameter [29], [30]. Farouki *et al.* [29] was the first to validate the use of PH splines on open CNC machines. Walton and Meek [30] has achieved  $G^2$  continuity by cubic and quintic PH splines. The tooltip position path length after using PH spline smoothing can be accurately and analytically calculated, and the calculation efficiency and accuracy are significantly improved compared with those of B-splines. However, the reason why PH splines have such an advantage is that the components of the PH spline derivative satisfy the Pythagorean theorem [31], [32]. A regular polynomial can only be transformed into a PH spline by first squaring its derivative and then integrating it. Therefore, the PH spline with the same continuous order has nearly twice as many control points as the B-spline, as shown in Fig. 1. The distribution of the positions of the control points is more complex than that of the B-spline, which makes the process of synchronisation more complex. Hu *et al.* [33] realised real-time  $C^3$  continuous corner smoothing and interpolation for five-axis machine tools by PH spline. An analytical synchronisation algorithm is developed to guarantee the motion variance of the smoothed tool orientation related to the tool tip displacement is also  $C^3$  continuous. Although synchronisation has been achieved in previous studies, robot tool end smoothing still encounters challenges.

The robot with six degrees of freedom (DOF) has an extra redundant degree around the tool axis, which can be optimised to achieve higher stiffness [34]–[37]. The extra redundant angle does not affect the tool pose in the WCS but influences the joint configuration of the robot [26], [38], [39]. To obtain continuous axis motion, the tooltip position, tool orientation, and redundant angle

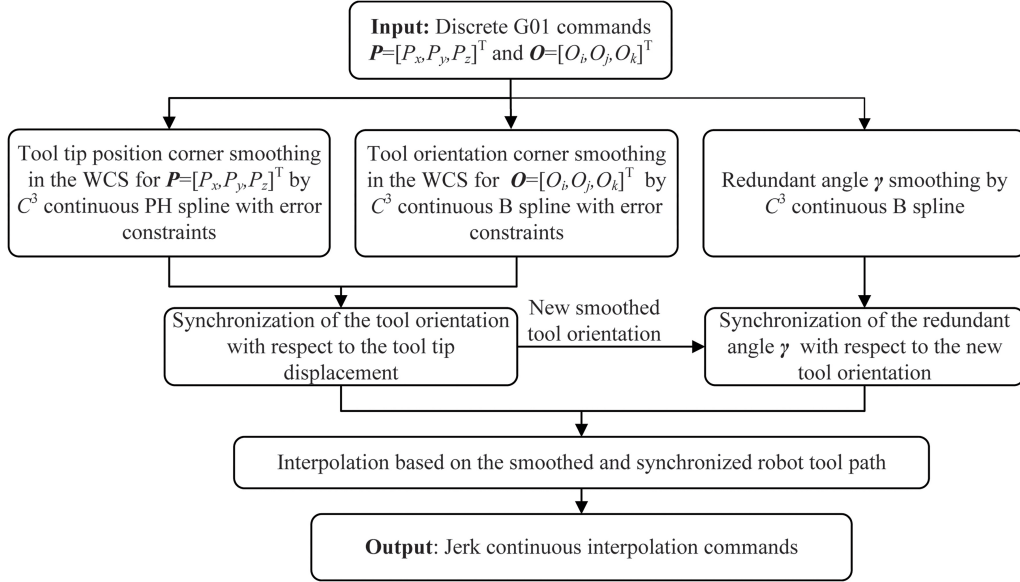


Figure 2. Flowchart of the proposed corner smoothing algorithm for robotic machining.

should all be smoothed for robotic machining. However, synchronisation among the three is quite difficult to achieve in the end.

To improve the accuracy and efficiency of robotic machining, this study proposes an innovative  $C^3$  continuous corner smoothing method with shape-preserving, redundant angle, and accurate real-time interpolations. The proposed method will fully utilise the advantages of the PH spline and B-spline to efficiently solve the problems of analytically calculating the path length of the smooth tooltip position and the error tolerance constraints and synchronising the tooltip position, tool orientation, and redundant angle, as shown in Fig. 2. First, to ensure accurate and real-time interpolation, only tooltip position corner is smoothed by the  $C^3$  continuous PH spline with the error tolerance constraint. Second, the tool orientation and redundant angle are smoothed by the  $C^3$  continuous B-spline, which has fewer control points and more efficient interpolation. Third, to guarantee the synchronisation of the three smoothed tool paths, a transitive synchronisation strategy is proposed. First, the tool orientation is synchronised with the tooltip position. Then, the redundant angle is synchronised with the tool orientation to achieve the goal of synchronising the redundant angle with the tooltip position. The details will be represented in the subsequent sections, which are organised as follows: Section 2 discusses the development of the analytical corner smoothing algorithm. Section 3 explores the analytical synchronisation algorithm. Section 4 presents the simulations and experiments conducted to verify the proposed method. Section 5 concludes the paper.

## 2. Analytical Corner Smoothing Algorithm with Redundant Angle for 6R Robot

The 6R robotic machining toolpath is generated by commercial computer-aided manufacturing software. The

machining tool path is formed by connecting the cutter location ( $[P_n, O_n]^T = [P_x, P_y, P_z, O_i, O_j, O_k]^T$   $n = 0, 1, 2, \dots$ ) in the WCS. The cutter location contains the tooltip position  $P = [P_x, P_y, P_z]^T$  expressed in the Cartesian coordinates and the tool orientation  $O = [O_i, O_j, O_k]^T$  expressed as the unit vector in the spherical coordinates. However, in the robotic machining system, a six-dimensional vector  $M = [x, y, z, \alpha, \beta, \gamma]^T$  represents the tool pose.  $[x, y, z]^T$  is the tooltip position that is the same as the tooltip position  $P = [P_x, P_y, P_z]^T$ , but  $[\alpha, \beta, \gamma]^T$  are  $z - y - z$  Euler angles. The cutter location in the WCS could be transferred to the tool pose of robotic machining by the transfer matrix, as follows:

$${}^wT = \text{Rot}(z, \alpha) \text{Rot}(y, \beta) \text{Rot}(z, \gamma) \text{Trans}(P_x, P_y, P_z), \quad (1)$$

$$\text{where } \text{Rot}(z, \alpha) = \begin{bmatrix} \cos \alpha & -\sin \alpha & 0 & 0 \\ \sin \alpha & \cos \alpha & 0 & 0 \\ 0 & 0 & 1 & 0 \\ 0 & 0 & 0 & 1 \end{bmatrix}, \quad \text{Rot}(y, \beta) =$$

$$\begin{bmatrix} \cos \beta & 0 & \sin \beta & 0 \\ 0 & 1 & 0 & 0 \\ -\sin \beta & 0 & \cos \beta & 0 \\ 0 & 0 & 0 & 1 \end{bmatrix}, \quad \text{Rot}(z, \gamma) = \begin{bmatrix} \cos \gamma & -\sin \gamma & 0 & 0 \\ \sin \gamma & \cos \gamma & 0 & 0 \\ 0 & 0 & 1 & 0 \\ 0 & 0 & 0 & 1 \end{bmatrix}, \quad \text{and}$$

$$\text{Trans}(P_x, P_y, P_z) = \begin{bmatrix} 1 & 0 & 0 & P_x \\ 0 & 1 & 0 & P_y \\ 0 & 0 & 1 & P_z \\ 0 & 0 & 0 & 1 \end{bmatrix}. \quad \text{Expanding (1) yields the}$$

relation between the tool orientation  $O = [O_i, O_j, O_k]^T$  and the Euler angles  $[\alpha, \beta, \gamma]^T$ , as follows:

$$O = [O_i, O_j, O_k]^T = [\cos \alpha \sin \beta, \sin \alpha \sin \beta, \cos \beta]^T. \quad (2)$$

According to (2), the Euler angle  $\gamma$  could be arbitrary and would not affect the tool orientation in the WCS. Therefore, the Euler angle  $\gamma$  is called the redundant DOF. However, for a cutter location with the Euler angle  $\gamma$ , the following unique corresponding robot configuration can be derived:

$$\theta(P, O, \gamma) = [\theta_1, \theta_2, \theta_3, \theta_4, \theta_5, \theta_6]^T \quad (3)$$

based on the closed-form inverse kinematic transformation.

In this study, a shape-preserving toolpath smoothing method is proposed to optimise the robotic machining trajectory, considering the error tolerance constraint, tool orientation, and redundant angle. The tooltip position, tool orientation, and redundant Euler angle  $\gamma$  are smoothed by the  $C^3$  continuous spline. To achieve real-time interpolation with velocity, acceleration, and jerk continuity of each axis, the tool orientation and redundant Euler angle  $\gamma$  need to be synchronised with the tooltip displacement. The details of the proposed corner smoothing and synchronisation method for the 6R robotic manipulator are presented in the subsections of this section.

## 2.1 Tooltip Position Corner Smoothing Algorithm

Because the robotic machine interpolator computes motion commands based on the given path length of the contour, the accurate computation of the smoothed tooltip position  $P = [P_x, P_y, P_z]^T$  is essential for robotic machining performance. In contrast to the Bezier/B-spline, the PH spline admits the analytic arc length by simply evaluating a polynomial. For an accurate interpolator, the PH spline is chosen to smooth the corner of the tooltip position corner in the WCS directly, as shown in Fig. 3.  $P_0, P_1, P_2$  are arbitrarily three consecutive tooltip positions in the WCS. Given two linear segments  $\overrightarrow{P_0P_1}$  and  $\overrightarrow{P_1P_2}$  that form a planar, to obtain a smooth jerk performance, a  $C^3$  planar PH spline is constructed. Because the synchronisation strategy proposed in Section 3 would not adjust the smoothing spline of the corner, the  $C^3$  PH spline is designed as symmetric, which can constrain the deviation precisely. In addition, the maximum deviation between the smoothed spline and the reference linear tooltip path occurs at the midpoint of the spline.

The  $C^3$  PH spline is expressed in the Bernstein form as follows:

$$r_p(u) = \sum_{i=0}^{11} A_i b_i^{11}(u), \quad u \in [0, 1], \quad (4)$$

where  $u$  is the spline parameter,  $b_i^{11}(u) = \frac{11!}{i!(11-i)!} u^i (1-u)^{11-i}$  is the basis function, and  $A_i$  is the control point. All control points of the symmetric  $C^3$  PH spline

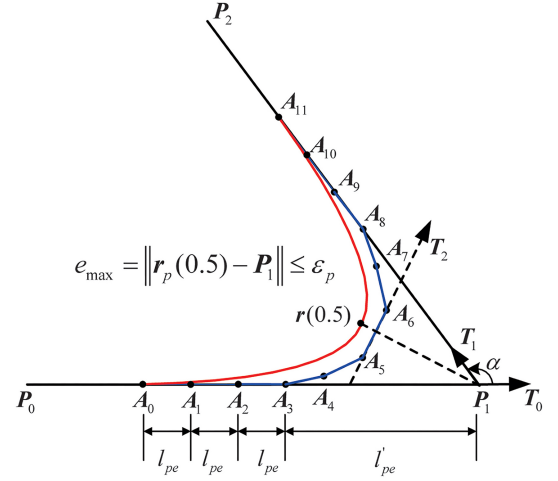


Figure 3. Corner smoothing of the tooltip position in the WCS.

were evaluated by [28] as follows:

$$\left\{ \begin{array}{l} A_0 = P_1 - (3l_{pe} + l'_{pe})\vec{T}_0 \\ A_1 = P_1 - (2l_{pe} + l'_{pe})\vec{T}_0 \\ A_2 = P_1 - (l_{pe} + l'_{pe})\vec{T}_0 \\ A_3 = P_1 - l'_{pe}\vec{T}_0 \\ A_4 = A_3 + \frac{5}{6}l_{pe}\vec{T}_0 + \frac{1}{6}l_{pe}\vec{T}_2 \\ A_5 = A_4 + \frac{10}{21}l_{pe}\vec{T}_0 + \frac{11}{21}l_{pe}\vec{T}_2 \\ A_6 = A_5 + l_{pe}\vec{T}_2 \\ A_7 = A_6 + \frac{10}{21}l_{pe}\vec{T}_1 + \frac{11}{21}l_{pe}\vec{T}_2 \\ A_8 = P_1 + l'_{pe}\vec{T}_1 \\ A_9 = P_1 + (l_{pe} + l'_{pe})\vec{T}_1 \\ A_{10} = P_1 + (2l_{pe} + l'_{pe})\vec{T}_1 \\ A_{11} = P_1 + (3l_{pe} + l'_{pe})\vec{T}_1, \end{array} \right. \quad (5)$$

where  $\vec{T}_0 = \frac{\overrightarrow{P_0P_1}}{\|\overrightarrow{P_0P_1}\|}$ ,  $\vec{T}_1 = \frac{\overrightarrow{P_1P_2}}{\|\overrightarrow{P_1P_2}\|}$ ,  $\vec{T}_2 = \frac{\vec{T}_0 + \vec{T}_1}{\|\vec{T}_0 + \vec{T}_1\|}$ ,  $l'_{pe} = \left( \frac{55}{42} + \frac{25}{21 \cos(\frac{\alpha}{2})} \right) l_{pe}$ , and  $\alpha = (\vec{T}_0 \cdot \vec{T}_1)$ . Then,  $\|\overrightarrow{A_0P_1}\|$  can be inferred as follows:

$$\|\overrightarrow{A_0P_1}\| = \|\overrightarrow{P_1A_{11}}\| = \left( \frac{181}{42} + \frac{25}{21 \cos(\frac{\alpha}{2})} \right) l_{pe}. \quad (6)$$

The length  $l_{pe}$  is constrained by the user-defined error tolerance ( $\varepsilon_p$ ). As shown in Fig. 3, the maximum smoothing deviation occurs at the midpoint of the inserted PH spline when the spline is symmetrical. The maximum smoothing deviation must be constrained as follows:

$$\|r(0.5) - P_1\| \leq \varepsilon_p. \quad (7)$$

According to (7) and referring to the study conducted by [28], the length  $l_{pe}$  is constrained by the user-defined error tolerance ( $\varepsilon_p$ ) as follows:

$$l_{pe} \leq \frac{\varepsilon_p}{\left(\frac{355}{672} + \frac{25}{21 \cos(\frac{\alpha}{2})}\right) \sin(\frac{\alpha}{2})}. \quad (8)$$

Given that the synchronisation strategy proposed in Section 3 requires a remaining linear segment between two splines of two adjacent corners, the maximum allowable lengths of the segments  $\|\overrightarrow{A_0P_1}\|$  and  $\|\overrightarrow{P_1A_{11}}\|$  are calculated as follows:

$$\begin{cases} \|\overrightarrow{A_0P_1}\| \leq \frac{\|\overrightarrow{P_0P_1}\|}{4} \\ \|\overrightarrow{P_1A_{11}}\| \leq \frac{\|\overrightarrow{P_1P_2}\|}{4} \end{cases}. \quad (9)$$

Combining the conditions expressed in (6), (8), and (9),  $l_{pe}$  is determined as follows:

$$l_{pe} = \min \left( \frac{10.5 \|\overrightarrow{P_0P_1}\|}{181 + \frac{50}{\cos(\frac{\alpha}{2})}}, \frac{10.5 \|\overrightarrow{P_1P_2}\|}{181 + \frac{50}{\cos(\frac{\alpha}{2})}}, \frac{\varepsilon_p}{\left(\frac{355}{672} + \frac{25}{21 \cos(\frac{\alpha}{2})}\right) \sin(\frac{\alpha}{2})} \right). \quad (10)$$

The function of the arc length of the  $C^3$  PH spline with respect to the parameter  $u$  is referred to in the study conducted by [28].

## 2.2 Tool Orientation Corner Smoothing Algorithm

In this study, the tool orientation is also smoothed in the WCS directly to constrain the deviation properly. Because the tool orientation  $O = [O_i, O_j, O_k]^T$  in the WCS is the orientation vector in a sphere, the tool orientation is smoothed in the spherical coordinates, as shown in Fig. 4.  $O_0, O_1, O_2$  are arbitrarily three consecutive tool orientations in the WCS, and the two linear segments  $\overrightarrow{O_0O_1}$  and  $\overrightarrow{O_1O_2}$  form a corner. Given that the arc length of the tool orientation microspline is not required when interpolating, the  $C^3$  B-spline, which has fewer control points, is chosen as the tool orientation smoothing spline. To constrain the tool orientation error, the  $C^3$  B-spline is first designed as symmetric.

To realise  $C^3$  continuous corner smoothing, the symmetric quintic B-spline with seven control points employed in the study of [40] is chosen to smooth the tool orientation. The symmetric quintic B-spline is expressed as follows:

$$r_O(u) = \sum_{i=0}^6 N_{i,6}(u) B_i, \quad u \in [0, 1], \quad (11)$$

where  $u$  is the spline parameter,  $B_i$  represents the control points, and  $N_{i,6}(u)$  is the basic function of the symmetric quintic B-spline. The basic function  $N_{i,6}(u)$  is recursively

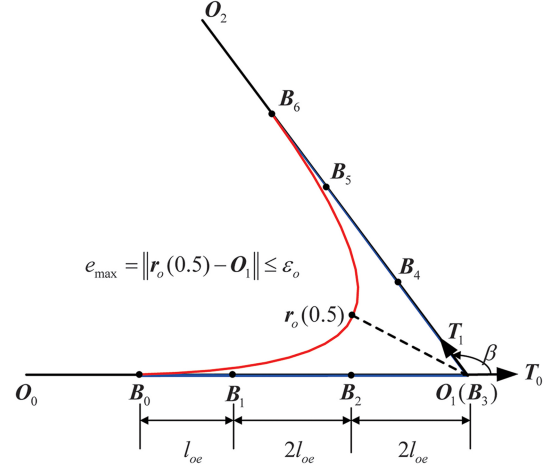


Figure 4. Corner smoothing of the tool orientation in the WCS.

defined with the knot vector  $U$ , as follows:

$$\begin{cases} U = [u_0, u_1, u_2, u_3, u_4, u_5, u_6, u_7, u_8, u_9, u_{10}, u_{11}, u_{12}]^T \\ = [0, 0, 0, 0, 0, 0, 0.5, 1, 1, 1, 1, 1, 1]^T \\ N_{i,6}(u) = \frac{u-u_i}{u_{i+5}-u_i} N_{i,5}(u) + \frac{u_{i+6}-u}{u_{i+6}-u_{i+1}} N_{i+1,5}(u) \quad 1 \\ N_{i,0}(u) = \begin{cases} 1, & u_i \leq u < u_{i+1} \\ 0, & \text{otherwise} \end{cases} \end{cases} \quad (12)$$

The position of the control point  $B_i$  satisfies the following expression:

$$\begin{cases} B_0 - B_1 = (B_1 - B_2) / 2, & B_1 - B_2 = B_2 - B_3 \\ B_6 - B_5 = (B_5 - B_4) / 2, & B_5 - B_4 = B_4 - B_3 \end{cases}. \quad (13)$$

Assuming the length of the control polygon  $\|\overrightarrow{B_0B_1}\| = l_{oa}$  and  $\|\overrightarrow{B_5B_6}\| = l_{ob}$ , the fourth control point  $B_3$  is chosen at the corner position  $O_1$ . Then, the other control points are obtained as follows:

$$\begin{cases} B_0 = O_1 - 5l_{oa}\vec{T}_0 \\ B_1 = O_1 - 4l_{oa}\vec{T}_0 \\ B_2 = O_1 - 2l_{oa}\vec{T}_0 \\ B_3 = O_1 \\ B_4 = O_1 + 2l_{ob}\vec{T}_1 \\ B_5 = O_1 + 4l_{ob}\vec{T}_1 \\ B_6 = O_1 + 5l_{ob}\vec{T}_1 \end{cases}, \quad \text{with } \vec{T}_0 = \frac{\overrightarrow{O_0O_1}}{\|\overrightarrow{O_0O_1}\|}, \vec{T}_1 = \frac{\overrightarrow{O_1O_2}}{\|\overrightarrow{O_1O_2}\|} \quad (14)$$

The values of  $l_{oa}$  and  $l_{ob}$  are evaluated based on the user-defined orientation error tolerance  $\varepsilon_o$  and synchronisation condition. The situation under the user-defined orientation error tolerance will be discussed in

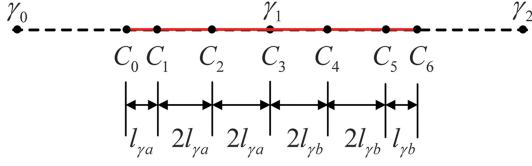


Figure 5. Smoothing of the redundant angle  $\gamma$ .

the subsequent paragraphs, and the situation under synchronisation will be explored in the subsequent subsection. Because of the symmetric quintic B-spline, the maximum smoothing deviation also occurs at the midpoint of the spline, and the maximum orientation error could be evaluated as follows:

$$\|O_1 - r_o(0.5)\| \leq \varepsilon_o. \quad (15)$$

Then, the values of  $l_{oa}$  and  $l_{ob}$  are constrained by the user-defined error tolerance ( $\varepsilon_o$ ) as follows:

$$l_{oe} \leq \frac{2\varepsilon_o}{3 \cos\left(\frac{\beta}{2}\right)}, \quad (16)$$

where  $\beta$  is the angle between  $\overrightarrow{O_0O_1}$  and  $\overrightarrow{O_1O_2}$ .

Given that the synchronisation strategy proposed in Section 3 requires a remaining linear segment between two splines of two adjacent corners, the maximum allowable lengths of the segments  $\|\overrightarrow{B_0O_1}\|$  and  $\|\overrightarrow{O_1B_6}\|$  are calculated as follows:

$$\begin{cases} \|\overrightarrow{B_0O_1}\| \leq \frac{\|\overrightarrow{O_0O_1}\|}{4} \\ \|\overrightarrow{O_1B_6}\| \leq \frac{\|\overrightarrow{O_1O_2}\|}{4}. \end{cases} \quad (17)$$

Combining the conditions expressed in (16) and (17),  $l_{oa}$  and  $l_{ob}$  are constrained as follows:

$$\begin{cases} l_{oa} \leq \min\left(\frac{\|\overrightarrow{O_0O_1}\|}{20}, \frac{2\varepsilon_o}{3 \cos\left(\frac{\beta}{2}\right)}\right) \\ l_{ob} \leq \min\left(\frac{\|\overrightarrow{O_1O_2}\|}{20}, \frac{2\varepsilon_o}{3 \cos\left(\frac{\beta}{2}\right)}\right). \end{cases} \quad (18)$$

The values of  $l_{oa}$  and  $l_{ob}$  would be finally determined by the synchronisation process in the subsequent subsection.

### 2.3 Redundant Angle $\gamma$ Smoothing Algorithm

The redundant angle  $\gamma$  is a scalar value. Although each  $\gamma$  has no corner, discrete angle  $\gamma$  still needs to be fitted with splines to achieve a smooth trajectory. Because the arc length of the redundant angle smoothing spline is not required when interpolating, the symmetric quintic B-spline with seven control points is also adopted to replace the transition part of the redundant angle. As shown in Fig. 5,  $\gamma_0, \gamma_1, \gamma_2$  are arbitrarily three consecutive redundant angles presented as three points on a straight line. A  $C^3$  B-spline is adopted to replace the transition part at the redundant angle  $\gamma_1$ .

The representation of the symmetric quintic B-spline for the redundant angle is the same as that of  $r_o(u)$ , expressed as follows:

$$r_\gamma(u) = \sum_{i=0}^6 N_{i,6}(u) C_i, \quad u \in [0, 1] \quad (19)$$

where  $u$  is the parameter of the spline,  $N_{i,6}(u)$  is the basic function, and  $C_i$  is the control point. The basic function  $N_{i,6}(u)$  is defined the same as the basic function of  $r_o(u)$ . In addition, the positions of the control points are also the same as those of  $r_o(u)$ , expressed as follows:

$$\begin{cases} C_0 - C_1 = (C_1 - C_2)/2, & C_1 - C_2 = C_2 - C_3 \\ C_6 - C_5 = (C_5 - C_4)/2, & C_5 - C_4 = C_4 - C_3. \end{cases} \quad (20)$$

If the fourth control point  $C_3$  is chosen at the corner position  $\gamma_1$ , then the other control points are obtained as follows:

$$\begin{cases} C_0 = \gamma_1 - 5l_{\gamma a} \text{sign}(\gamma_1 - \gamma_0) \\ C_1 = \gamma_1 - 4l_{\gamma a} \text{sign}(\gamma_1 - \gamma_0) \\ C_2 = \gamma_1 - 2l_{\gamma a} \text{sign}(\gamma_1 - \gamma_0) \\ C_3 = \gamma_1 \\ C_4 = \gamma_1 + 2l_{\gamma b} \text{sign}(\gamma_2 - \gamma_1) \\ C_5 = \gamma_1 + 4l_{\gamma b} \text{sign}(\gamma_2 - \gamma_1) \\ C_6 = \gamma_1 + 5l_{\gamma b} \text{sign}(\gamma_2 - \gamma_1). \end{cases}, \text{ with} \quad (21)$$

$$\begin{cases} \text{sign}(\gamma_i - \gamma_{i-1}) = 1, & \text{if } \gamma_i > \gamma_{i-1} \\ \text{sign}(\gamma_i - \gamma_{i-1}) = -1, & \text{if } \gamma_i < \gamma_{i-1} \end{cases}.$$

Because the redundant angle  $\gamma$  is a scalar value and has no impact on the tool path, a smoothing deviation is not required to constrain the lengths  $l_{\gamma a}$  and  $l_{\gamma b}$ . To synchronise with the tooltip position, the maximum allowable lengths of the segments  $\|\overrightarrow{C_0\gamma_1}\|$  and  $\|\overrightarrow{\gamma_1 C_6}\|$  are calculated as follows:

$$\begin{cases} \|\overrightarrow{C_0\gamma_1}\| \leq \frac{\|\overrightarrow{\gamma_0\gamma_1}\|}{4} \\ \|\overrightarrow{\gamma_1 C_6}\| \leq \frac{\|\overrightarrow{\gamma_1\gamma_2}\|}{4}. \end{cases} \quad (22)$$

Thus, the lengths  $l_{\gamma a}$  and  $l_{\gamma b}$  are limited to:

$$l_{\gamma a} \leq \frac{\|\overrightarrow{\gamma_0\gamma_1}\|}{20} \quad \text{and} \quad l_{\gamma b} \leq \frac{\|\overrightarrow{\gamma_1\gamma_2}\|}{20}. \quad (23)$$

In summary, the symmetric quintic B-spline  $r_\gamma(u)$  could be obtained if the values of  $l_{\gamma a}$  and  $l_{\gamma b}$  are known. However, the values of  $l_{\gamma a}$  and  $l_{\gamma b}$  are evaluated based on the synchronisation condition, which will be explored in the subsequent section.

### 3. Transitive Synchronisation Algorithm

To achieve jerk continuous axis motion, the first-order, second-order, and third-order derivatives of the tool orientation vectors with respect to the tooltip displacement

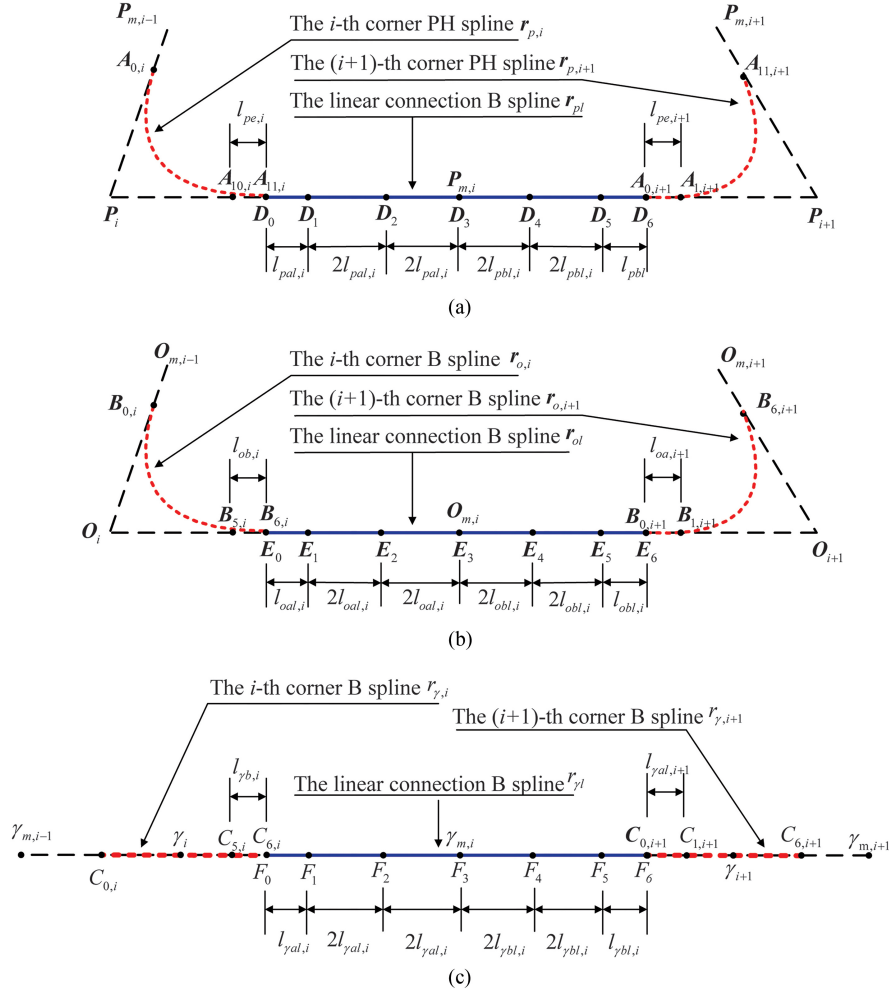


Figure 6. Proposed synchronisation strategy by  $C^3$  continuous connection for (a) the tool tip position, (b) the tool orientation, and (c) the redundant angle.

should be continuous at the junctions. As shown in Fig. 6,  $\overrightarrow{A_{11,i}A_{0,i+1}}$ ,  $\overrightarrow{B_{7,i}B_{0,i+1}}$ , and  $\overrightarrow{C_{7,i}C_{0,i+1}}$  are the remaining linear segments after smoothing, which are between two adjacent smooth splines.

If synchronisation is ensured by adjusting the corner smoothing spline, then two problems will arise. The corner smoothing error becomes smaller under error tolerance, which results in a greater curvature at the corners, leading to a reduction in the machining feed at the corners. In addition, adjusting the corner smoothing spline affects the length of the remaining linear segment, leading to difficulties in global synchronisation.

For these reasons, this study first synchronises the three splines at the corner with the midpoint  $P_{m,i}$ ,  $O_{m,i}$ ,  $\gamma_{m,i}$  of each straight-line segment of the original path as the boundary and then constructs a  $C^3$  B-spline replacing all of the remaining linear segments of the smoothed tooltip position, tool orientation, and redundant angle. The linear  $C^3$  B-spline connects two adjacent microsplines as if they are joined hand in hand. We assumed that the linear spline of the tooltip position, tool orientation, and redundant angle are expressed as  $r_{pl}(u)$ ,  $r_{ol}(u)$ , and  $r_{\gamma l}(u)$ , respectively, as shown in Fig. 6. Even though the B-spline has no analytical solution of the

arc-length, we calculate the length of the linear B-spline by calculating the length between two endpoints of the linear segment.

Corner synchronisation is conducted within the corner range, with the midpoint  $P_{m,i}$ ,  $O_{m,i}$ ,  $\gamma_{m,i}$  of each straight-line segment of the original path as the boundary, as shown in Fig. 6. To ensure that the varying rates of the tool orientation and redundant angle  $\gamma$  with respect to the tooltip displacement are both  $C^3$  continuous at the junctions, the first-order, second-order, and third-order derivatives of the tool orientation vectors and redundant angle  $\gamma$  with respect to the tooltip displacement should be continuous at the junctions. Taking the three corners  $\angle P_{m,i-1}P_iP_{m,i}$ ,  $\angle O_{m,i-1}O_iO_{m,i}$ , and  $\angle \gamma_{m,i-1}\gamma_i\gamma_{m,i}$  as an example, the corresponding corner splines are denoted as  $r_{p,i}$ ,  $r_{o,i}$ , and  $r_{\gamma,i}$ , respectively. The corner synchronisation condition could be expressed as follows:

$$\left\{ \begin{array}{l} \frac{dr_{o,i}}{ds} \Big|_{u=0} = \frac{\overrightarrow{O_{m,i-1}B_{0,i}}}{\|\overrightarrow{P_{m,i-1}A_{0,i}}\|}, \quad \frac{dr_{o,i}}{ds} \Big|_{u=1} = \frac{\overrightarrow{B_{6,i}O_{m,i}}}{\|\overrightarrow{A_{11,i}P_{m,i}}\|} \\ \frac{d^2r_{o,i}}{ds^2} \Big|_{u=0,1} = 0, \quad \frac{d^3r_{o,i}}{ds^3} \Big|_{u=0,1} = 0 \\ \frac{dr_{\gamma,i}}{ds} \Big|_{u=0} = \frac{\overrightarrow{\gamma_{m,i-1}C_{0,i}}}{\|\overrightarrow{P_{m,i-1}A_{0,i}}\|}, \quad \frac{dr_{\gamma,i}}{ds} \Big|_{u=1} = \frac{\overrightarrow{C_{6,i}\gamma_{m,i}}}{\|\overrightarrow{A_{11,i}P_{m,i}}\|} \\ \frac{d^2r_{\gamma,i}}{ds^2} \Big|_{u=0,1} = 0, \quad \frac{d^3r_{\gamma,i}}{ds^3} \Big|_{u=0,1} = 0. \end{array} \right. \quad (24)$$

Given the following relation:

$$\begin{cases} \frac{dr_{o,i}}{ds} \Big|_{u=0} = \frac{dr_{o,i}}{du} \frac{du}{ds} \Big|_{u=0} = \frac{10l_{oa,i}}{11l_{pe,i}} \\ \frac{dr_{o,i}}{ds} \Big|_{u=1} = \frac{dr_{o,i}}{du} \frac{du}{ds} \Big|_{u=1} = \frac{10l_{ob,i}}{11l_{pe,i}} \\ \frac{dr_{\gamma,i}}{ds} \Big|_{u=0} = \frac{dr_{\gamma,i}}{du} \frac{du}{ds} \Big|_{u=0} = \frac{10l_{\gamma a,i}}{11l_{pe,i}} \\ \frac{dr_{\gamma,i}}{ds} \Big|_{u=1} = \frac{dr_{\gamma,i}}{du} \frac{du}{ds} \Big|_{u=1} = \frac{10l_{\gamma b,i}}{11l_{pe,i}} \end{cases} \quad (25)$$

the corner synchronisation condition expressed in (24) could be rewritten as follows:

$$\begin{cases} \frac{10l_{oa,i}}{11l_{pe,i}} = \frac{\|\overrightarrow{O_{m,i-1}B_{0,i}}\|}{\|\overrightarrow{P_{m,i-1}A_{0,i}}\|}, & \frac{10l_{ob,i}}{11l_{pe,i}} = \frac{\|\overrightarrow{B_{6,i}O_{m,i}}\|}{\|\overrightarrow{A_{11,i}P_{m,i}}\|} \\ \frac{10l_{\gamma a,i}}{11l_{pe,i}} = \frac{\|\overrightarrow{\gamma_{m,i-1}C_{0,i}}\|}{\|\overrightarrow{P_{m,i-1}A_{0,i}}\|}, & \frac{10l_{\gamma b,i}}{11l_{pe,i}} = \frac{\|\overrightarrow{C_{6,i}\lambda_{m,i}}\|}{\|\overrightarrow{A_{11,i}P_{m,i}}\|} \end{cases} \quad (26)$$

Based on (26), the equivalent corner synchronisation condition could be derived as follows:

$$\begin{cases} \frac{10l_{oa,i}}{11l_{pe,i}} = \frac{\|\overrightarrow{O_{m,i-1}B_{0,i}}\|}{\|\overrightarrow{P_{m,i-1}A_{0,i}}\|}, & \frac{10l_{ob,i}}{11l_{pe,i}} = \frac{\|\overrightarrow{B_{6,i}O_{m,i}}\|}{\|\overrightarrow{A_{11,i}P_{m,i}}\|} \\ \frac{l_{\gamma a,i}}{l_{oa,i}} = \frac{\|\overrightarrow{\gamma_{m,i-1}C_{0,i}}\|}{\|\overrightarrow{O_{m,i-1}B_{0,i}}\|}, & \frac{l_{\gamma b,i}}{l_{ob,i}} = \frac{\|\overrightarrow{C_{6,i}\gamma_{m,i}}\|}{\|\overrightarrow{B_{6,i}O_{m,i}}\|} \end{cases} \quad (27)$$

According to (27), the proposed synchronisation method is derived as transitive as the smoothed tool orientation should be synchronised with the tooltip position, and the redundant angle should be synchronised with the new tool orientation.

### 3.1 Synchronisation of the Tool Orientation with Respect to the Tooltip Displacement

From the equivalent corner synchronisation condition expressed in (27), the corner synchronisation of the tool orientation with respect to the tooltip position displacement is expressed as follows:

$$\begin{cases} \frac{10l_{oa,i}}{11l_{pe,i}} = \frac{\|\overrightarrow{O_{m,i-1}B_{0,i}}\|}{\|\overrightarrow{P_{m,i-1}A_{0,i}}\|} = \frac{\|\overrightarrow{O_{m,i-1}O_i} - \|\overrightarrow{B_{0,i}O_i}\|}{\|\overrightarrow{P_{m,i-1}P_i} - \|\overrightarrow{A_{0,i}P_i}\|} \\ \frac{10l_{ob,i}}{11l_{pe,i}} = \frac{\|\overrightarrow{B_{6,i}O_{m,i}}\|}{\|\overrightarrow{A_{11,i}P_{m,i}}\|} = \frac{\|\overrightarrow{O_iO_{m,i}} - \|\overrightarrow{O_iB_{6,i}}\|}{\|\overrightarrow{P_iP_{m,i}} - \|\overrightarrow{P_iA_{11,i}}\|} \end{cases} \quad (28)$$

Referring to the positions of the control points discussed in Section 2, the values of  $l_{oa,i}$  and  $l_{ob,i}$  could be determined as follows:

$$\begin{cases} l_{oa,i} = \frac{1.1l_{pe,i} \|\overrightarrow{O_{m,i-1}O_i}\|}{\|\overrightarrow{P_{m,i-1}P_i}\| + \frac{25}{21} \left(1 - \frac{1}{21 \cos(\alpha_i/2)}\right) l_{pe,i}} \\ l_{ob,i} = \frac{1.1l_{pe,i} \|\overrightarrow{O_iO_{m,i+1}}\|}{\|\overrightarrow{P_iP_{m,i+1}}\| + \frac{25}{21} \left(1 - \frac{1}{21 \cos(\alpha_i/2)}\right) l_{pe,i}} \end{cases} \quad (29)$$

In addition, the values of  $l_{oa,i}$  and  $l_{ob,i}$  should be smaller than that of  $l_{oe,i}$  to guarantee the smoothing deviation under the error tolerance constraint  $\varepsilon_o$  for the tool orientation path. Thus,  $l_{pe,i}$  should be further

constrained as follows:

$$l_{pe,i} = \min \left( \frac{21 \|\overrightarrow{P_{m,i-1}P_i}\|}{181 + \frac{50}{\cos(\frac{\alpha_i}{2})}}, \frac{21 \|\overrightarrow{P_iP_{m,i}}\|}{181 + \frac{50}{\cos(\frac{\alpha_i}{2})}} \right), \quad (30)$$

$$\frac{\varepsilon_p}{\left(\frac{355}{672} + \frac{25}{21 \cos(\frac{\alpha_i}{2})}\right) \sin(\frac{\alpha_i}{2})},$$

$$\frac{l_{oe} \|\overrightarrow{P_{m,i-1}P_i}\|}{\frac{11}{10} \|\overrightarrow{O_{m,i-1}O_i}\| - \frac{25}{21} \left(1 - \frac{1}{21 \cos(\alpha_i/2)}\right) l_{oe,i}},$$

$$\frac{l_{oe} \|\overrightarrow{P_iP_{m,i}}\|}{\frac{11}{10} \|\overrightarrow{O_iO_{m,i}}\| - \frac{25}{21} \left(1 - \frac{1}{21 \cos(\alpha_i/2)}\right) l_{oe,i}} \Bigg) \quad (30)$$

Thus, the appropriate value of  $l_{pe,i}$  is determined according to (30) and the corresponding values of  $l_{oa,i}$  and  $l_{ob,i}$  are determined according to (29). The determined values of  $l_{pe,i}$ ,  $l_{oa,i}$ , and  $l_{ob,i}$  would guarantee that the tool orientation is synchronised with the tooltip displacement under the error tolerance constraints  $\varepsilon_p$  and  $\varepsilon_o$  in the corner.

### 3.2 Synchronisation of the Redundant Angle $\gamma$ with Respect to the New Tool Orientation

The redundant angle  $\gamma$  and new tool orientation within corner ranges are synchronised with the midpoint of each straight-line segment of the original path as the boundary, as shown in Fig. 6. Combined with (27), the corner synchronisation condition of the redundant angle  $\gamma$  with respect to the new tool orientation is expressed as follows:

$$\begin{cases} \frac{l_{\gamma a,i}}{l_{oa,i}} = \frac{\|\overrightarrow{\gamma_{m,i-1}C_{0,i}}\|}{\|\overrightarrow{O_{m,i-1}B_{0,i}}\|} = \frac{\|\overrightarrow{\gamma_{m,i-1}\gamma_i} - \|\overrightarrow{C_{0,i}\gamma_i}\|}{\|\overrightarrow{O_{m,i-1}O_i} - \|\overrightarrow{B_{0,i}O_i}\|} \\ \frac{l_{\gamma b,i}}{l_{ob,i}} = \frac{\|\overrightarrow{C_{6,i}\gamma_{m,i}}\|}{\|\overrightarrow{B_{6,i}O_{m,i}}\|} = \frac{\|\overrightarrow{\gamma_i\gamma_{m,i}} - \|\overrightarrow{\gamma_iC_{6,i}}\|}{\|\overrightarrow{O_iO_{m,i}} - \|\overrightarrow{O_iB_{6,i}}\|} \end{cases} \quad (31)$$

In addition,  $\|\overrightarrow{C_{0,i}\gamma_i}\| = 5l_{\gamma a,i}$ ,  $\|\overrightarrow{\gamma_iC_{6,i}}\| = 5l_{\gamma b,i}$ ,  $\|\overrightarrow{B_{0,i}O_i}\| = 5l_{oa,i}$ ,  $\|\overrightarrow{O_iB_{6,i}}\| = 5l_{ob,i}$  combined with the determined values of  $l_{oa,i}$  and  $l_{ob,i}$  based on (29), the values of  $l_{\gamma a,i}$  and  $l_{\gamma b,i}$  are obtained as follows:

$$l_{\gamma a,i} = \frac{\|\overrightarrow{\gamma_{m,i-1}\gamma_i}\| l_{oa,i}}{\|\overrightarrow{O_{m,i-1}O_i}\|}, \quad l_{\gamma b,i} = \frac{\|\overrightarrow{\gamma_i\gamma_{m,i}}\| l_{ob,i}}{\|\overrightarrow{O_iO_{m,i}}\|} \quad (32)$$

### 3.3 $C^3$ Continuous Connection between Two Adjacent Inserted Microsplines

Corner synchronisation can only ensure continuous synchronisation at the intersection point between the inserted spline and the remaining linear segment within a single corner. The remaining linear segment connects two corner splines and is affected by the length of the two adjacent splines. Given that the three corner splines are synchronised in the corresponding corner, a  $C^3$  continuous linear spline needs to be adopted to replace the remaining linear segment. The  $C^3$  continuous linear spline connects

two adjacent corner splines to obtain global continuity. The first-order, second-order, and third-order derivatives at the conjunction should be equal to the corner synchronisation condition expressed in (27).

The control point of the symmetric quintic B-spline can be adjusted easily, and the length of the linear spline can be calculated based on the distance between two points. Thus, this study adopted the same symmetric quintic B-spline as  $r_o(u)$  to replace the remaining linear segment of the corner smoothed tooltip position, tool orientation, and redundant angle as follows:

$$\begin{cases} r_{p1}(\xi) = \sum_{i=0}^6 N_{i,6}(\xi) D_i \\ r_{o1}(\xi) = \sum_{i=0}^6 N_{i,6}(\xi) E_i, \quad \xi \in [0, 1] \\ r_{\gamma1}(\xi) = \sum_{i=0}^6 N_{i,6}(\xi) F_i, \end{cases} \quad (33)$$

where  $\xi$  is the parameter of the spline,  $N_{i,6}(\xi)$  is the basic function, and  $D_i, E_i$ , and  $F_i$  are the control points. The basic function  $N_{i,6}(\xi)$  is defined the same as the basic function of  $r_o(\xi)$ . In addition, the relative position of the control points is also the same as that of  $r_o(\xi)$ , expressed as follows:

$$\begin{cases} D_0 - D_1 = (D_1 - D_2)/2, & D_1 - D_2 = D_2 - D_3 \\ D_6 - D_5 = (D_5 - D_4)/2, & D_5 - D_4 = D_4 - D_3 \end{cases}. \quad (34)$$

The relative positions of control points  $E_i$  and  $F_i$  are the same as that of control point  $D_i$ , as shown in Fig. 6. To connect the microsplines in the corners with the  $C^3$  continuous linear spline, the three linear splines should guarantee the following condition:

$$\begin{cases} \frac{dr_{o1}}{ds}|_{\xi=0} = \frac{\| \overrightarrow{B_{6,i}O_{m,i}} \|}{\| \overrightarrow{A_{11,i}P_{m,i}} \|}, & \frac{dr_{o1}}{ds}|_{\xi=1} = \frac{\| \overrightarrow{O_{m,i}B_{0,i+1}} \|}{\| \overrightarrow{P_{m,i}A_{0,i+1}} \|} \\ \frac{dr_{\gamma1}}{ds}|_{\xi=0} = \frac{\| \overrightarrow{C_{6,i}\gamma_{m,i}} \|}{\| \overrightarrow{A_{11,i}P_{m,i}} \|}, & \frac{dr_{\gamma1}}{ds}|_{\xi=1} = \frac{\| \overrightarrow{\gamma_{m,i}C_{0,i+1}} \|}{\| \overrightarrow{P_{m,i}A_{0,i+1}} \|}. \end{cases} \quad (35)$$

Given that  $\frac{dr_{o1}}{ds}|_{\xi=0} = \frac{l_{oal}}{l_{pal}}$ ,  $\frac{dr_{o1}}{ds}|_{\xi=1} = \frac{l_{obl}}{l_{pbl}}$ ,  $\frac{dr_{\gamma1}}{ds}|_{\xi=0} = \frac{l_{\gamma al}}{l_{\gamma bl}}$ , and  $\frac{dr_{\gamma1}}{ds}|_{\xi=1} = \frac{l_{\gamma bl}}{l_{pbl}}$ , as shown in Fig. 6, the lengths of  $l_{pal}, l_{pbl}, l_{oal}, l_{obl}, l_{\gamma al}$ , and  $l_{\gamma bl}$  could be determined as follows:

$$\begin{cases} l_{pal} = \frac{\| \overrightarrow{A_{11,i}P_{m,i}} \|}{5}, & l_{pbl} = \frac{\| \overrightarrow{P_{m,i}A_{0,i+1}} \|}{5} \\ l_{oal} = \frac{\| \overrightarrow{B_{6,i}O_{m,i}} \|}{5}, & l_{obl} = \frac{\| \overrightarrow{O_{m,i}B_{0,i+1}} \|}{5} \\ l_{\gamma al} = \frac{\| \overrightarrow{C_{6,i}\gamma_{m,i}} \|}{5}, & l_{\gamma bl} = \frac{\| \overrightarrow{\gamma_{m,i}C_{0,i+1}} \|}{5}. \end{cases} \quad (36)$$

#### 4. Simulations and Experiments

The proposed global  $C^3$  tool path smoothing algorithm for robotic machining is verified by simulations and experiments in this section. The simulations are implemented with MATLAB 2020, which is installed in a laptop (Intel® Core™ i7-8565U CPU @ 1.80 GHz 1.99 GHz, 64-bit operating system). The experiments are conducted with an HSRCo610 robot, as shown in Fig. 7.

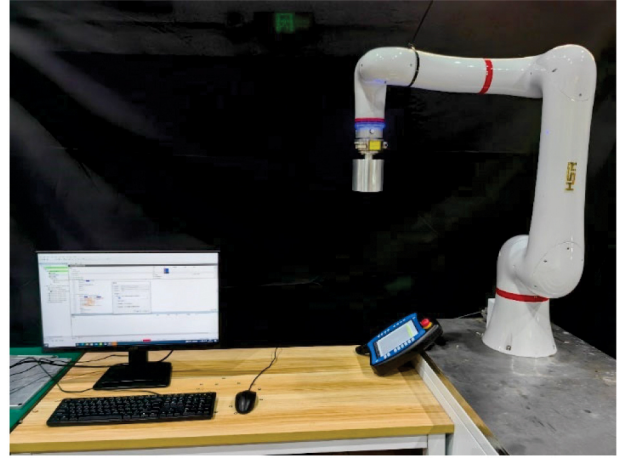


Figure 7. Experimental setup.

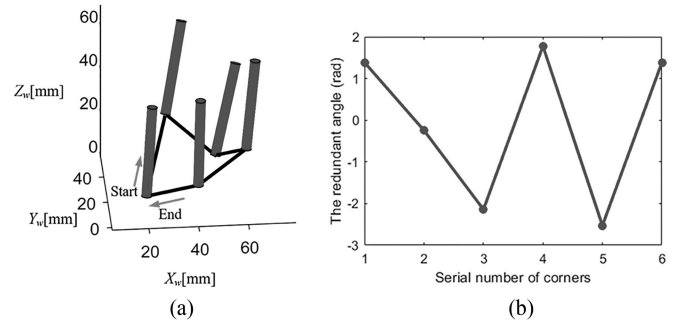


Figure 8. Discrete cutter location commands of (a) tool pose and (b) the redundant angle.

#### 4.1 Simulations

The testing tool path with sharp corners is shown in Fig. 8. The input discrete cutter location commands include the tooltip position  $P = [P_x, P_y, P_z]^T$  and tool orientation  $O = [O_i, O_j, O_k]^T$  in the WCS, as shown in Fig. 8(a). The reference command of the redundant angle is shown in Fig. 8(b). The reference tool path consists of six discrete tool poses and is a closed tool path. The machining process from the starting point to the ending point would pass through four corners.

The error tolerance constraints of the tooltip position and tool orientation are set as  $\varepsilon_p = 0.05$  mm and  $\varepsilon_o = 0.2$  mrad, respectively. Because the redundant angle is a one-dimensional vector, there is no smoothing error for it. The tool path smoothing effect is presented in Fig. 9.

The real maximum deviation of each tooltip position corner and tool orientation corner is shown in Fig. 10. Tooltip position smoothing and tool orientation smoothing can constrain the deviation error within the error tolerance. In addition, the deviations are not undersized because of synchronisation.

To demonstrate that the proposed method can ensure the third-order synchronisation of the redundant angle and tool orientation with the tooltip position, this study simulates the synchronisation situation of the starting and ending points of the smoothed corner. The synchronisation

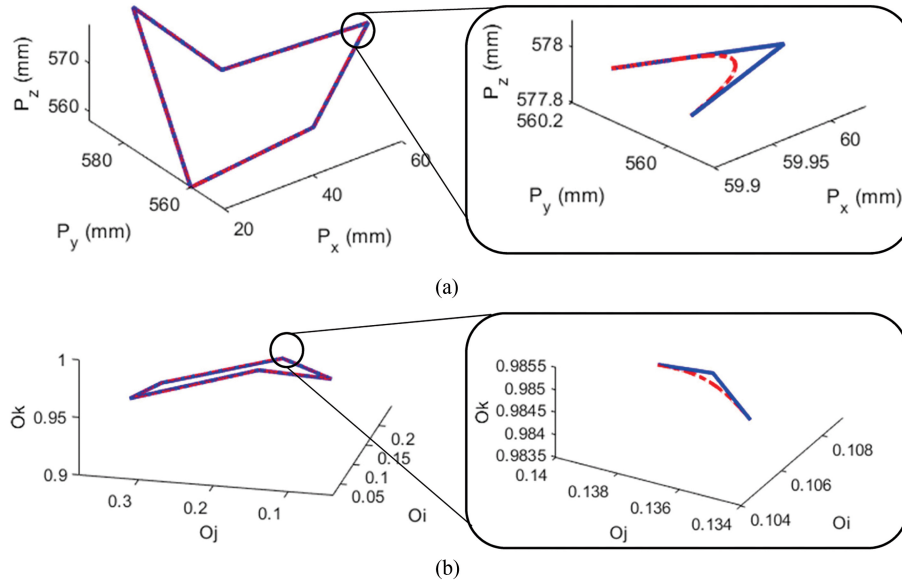


Figure 9. Corner smoothing results of (a) the tooltip position and (b) the tool orientation ( $\epsilon_p = 0.05$  mm and  $\epsilon_o = 0.2$  mrad).

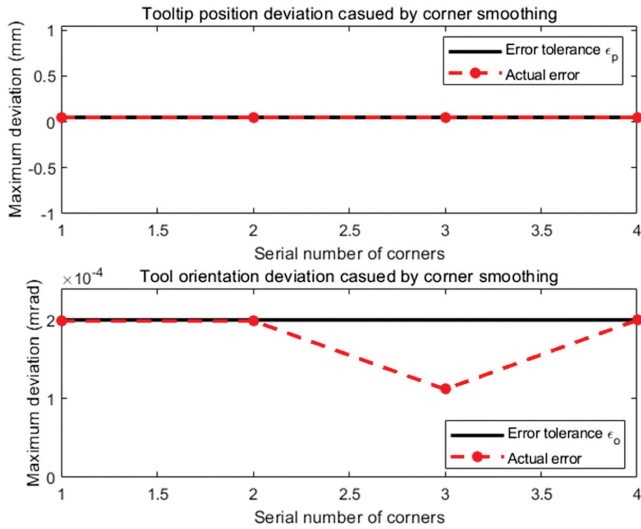


Figure 10. Maximum deviation of the smoothed tool path.

error between the linear spline segment and the corner micro spline is shown in Fig. 11. Notably, the first-, second-, and third-order synchronisation errors are all near zero, indicating that the proposed smoothing method can guarantee third-order synchronisation of the redundant angle and tool orientation with respect to the tooltip position.

Given the third-order synchronisation of the redundant angle and tool orientation with the tooltip position, the jerk continuous trajectory of all axes could be obtained after interpolation and inverse kinematic transformation. The existing study of 6R robotic tool path corner smoothing methods struggled with the synchronisation of the tool orientation with the tooltip position under the smoothing error tolerance. The redundant angle is considered a fixed value. However, the adjustment of redundant angles can improve robot stiffness. To achieve high machining accuracy, the redundant angle should be utilised, but its

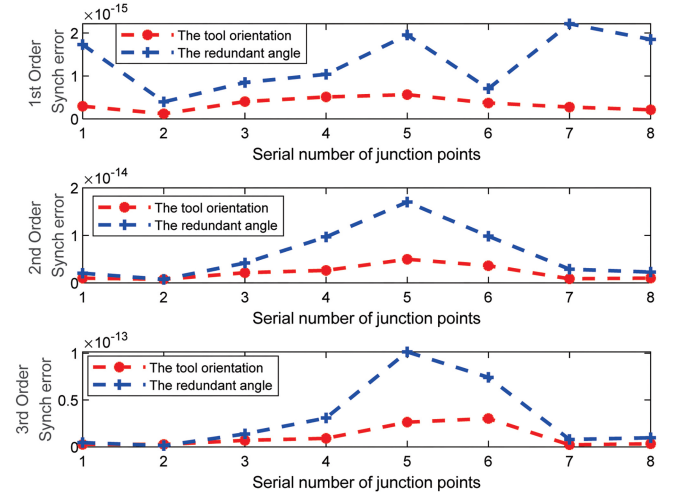


Figure 11. The synchronisation error.

value should not be fixed. In this situation, the existing relative study did not consider the redundant angle, which would cause non-smooth motion commands even through tooltip position and tool orientation smoothing.

The smoothing strategy without considering the redundant angle and the proposed method implemented with varying redundant angles are compared. The original discrete tool path shown in Fig. 8 is used for comparison. Based on the stiffness optimisation method, the corresponding redundant angle is generated. The error tolerance constraints of the tooltip position and tool orientation smoothing are set as  $\epsilon_p = 0.5$  mm and  $\epsilon_o = 0.02$  mrad, respectively. The tangential feedrate ( $F$ ), maximum acceleration ( $A_{max}$ ), and jerk ( $J_{max}$ ) are set as 25 mm/s, 500 mm/s<sup>2</sup>, and 2,000 mm/s<sup>3</sup>, respectively. The period of interpolation is set as 4 ms. The jerks of all six axes are shown in Fig. 12. The discontinuous redundant angle could cause a sudden change in the jerk of all axes. The jerks of all axes are continuous along the entire path

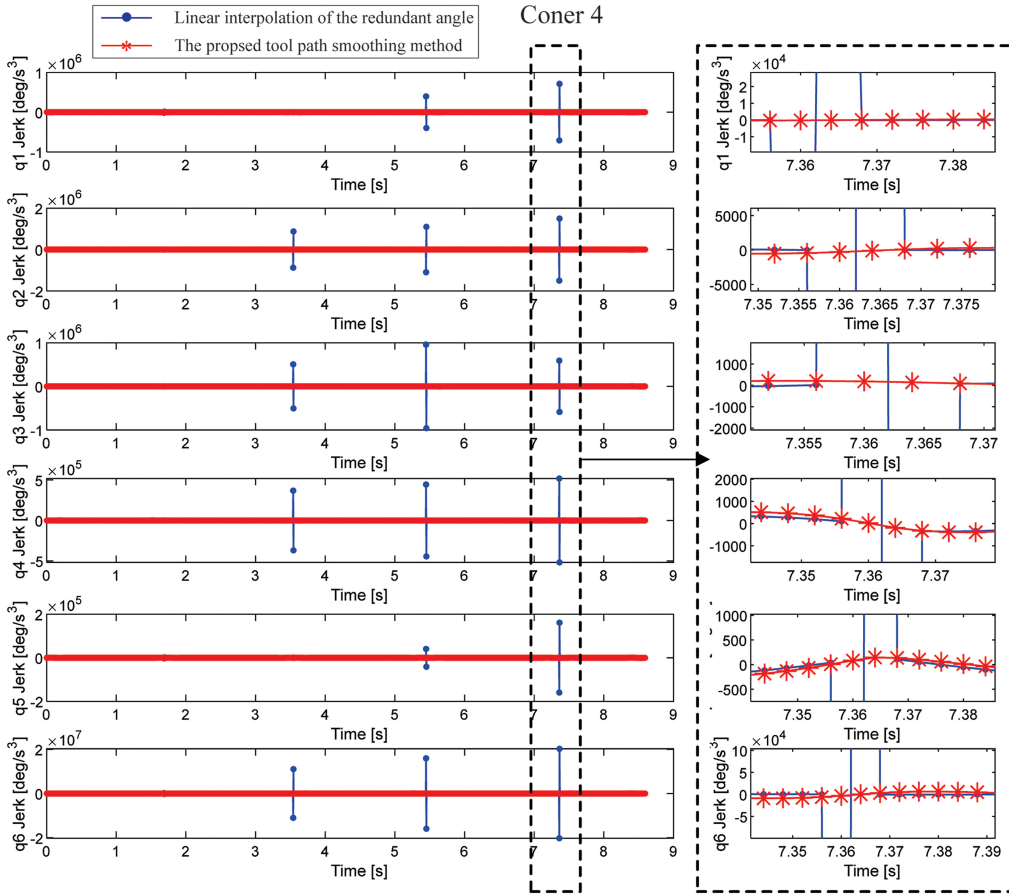


Figure 12. Comparison of jerk continuous joint commands.

Table 1  
Comparison of the Tracking Error RMSE of the Two Methods

Method	The RMSE of the Tracking Error (rad)					
	Joint1	Joint2	Joint3	Joint4	Joint5	Joint6
Linear interpolation of the redundant anlg	0.0149	0.025	0.0179	0.0215	0.0142	0.3041
The proposed method	0.0115	0.0136	0.0117	0.0194	0.0130	0.1607
Reduction (%)	22.8%	45.6%	34.6%	9.7%	8.4%	47.2%

by the proposed tool path smoothing method, and the proposed method has been verified to guarantee global  $C^3$  continuity.

## 4.2 Experiments

The proposed 6R robot tool path smoothing method is evaluated with the experimental setup shown in Fig. 7. The model of the robot is HSRCo610 with an interpolation period of 4 ms. The error tolerance constraints of the tooltip position and tool orientation smoothing are set as  $\varepsilon_p = 0.5$  mm and  $\varepsilon_o = 0.02$  mrad, respectively. The tangential feedrate ( $F$ ), maximum acceleration ( $A_{\max}$ ), and jerk ( $J_{\max}$ ) are set as 25 mm/s, 500 mm/s<sup>2</sup>, and 2,000 mm/s<sup>3</sup>, respectively. In the experiments, the joint commands generated by the smoothing strategy without considering the redundant angle and the proposed method

are executed with the HSRCo610 robot. The tracking errors of each axis are compared in Fig. 13. Notably, the tracking errors of the joint positions are nearly reduced by the proposed method. The the root mean square error (RMSE) of the tracking errors of the corresponding joint commands are evaluated and compared in Table 1. The tracking error RMSE of joints are all reduced by the proposed method, which has better performance. The decrease in the tracking errors of the corresponding joint commands is evaluated and presented in Fig. 14. The large decrease in tracking errors occurred at the corners, and the maximum decrease in tracking errors could reach 100%. The results showed that the proposed smoothing method of the tooltip position, tool orientation, and redundant angle of the 6R robotic machining with synchronisation could significantly reduce the tracking error of each axis, which can improve the robotic machining performance.

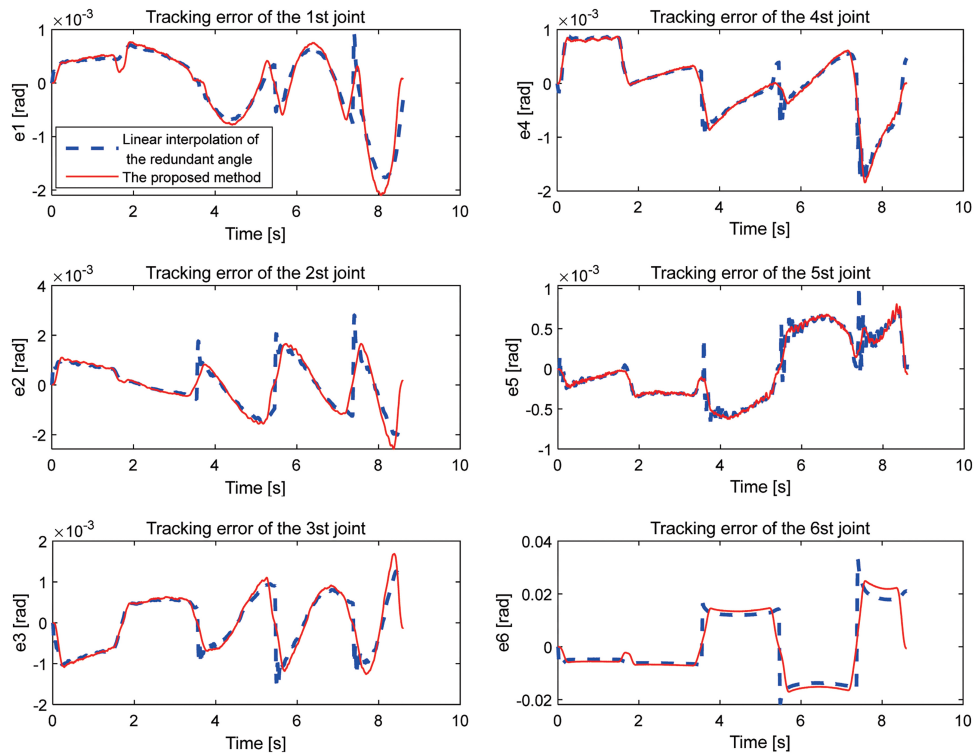


Figure 13. Tracking error of each axis with the two methods.

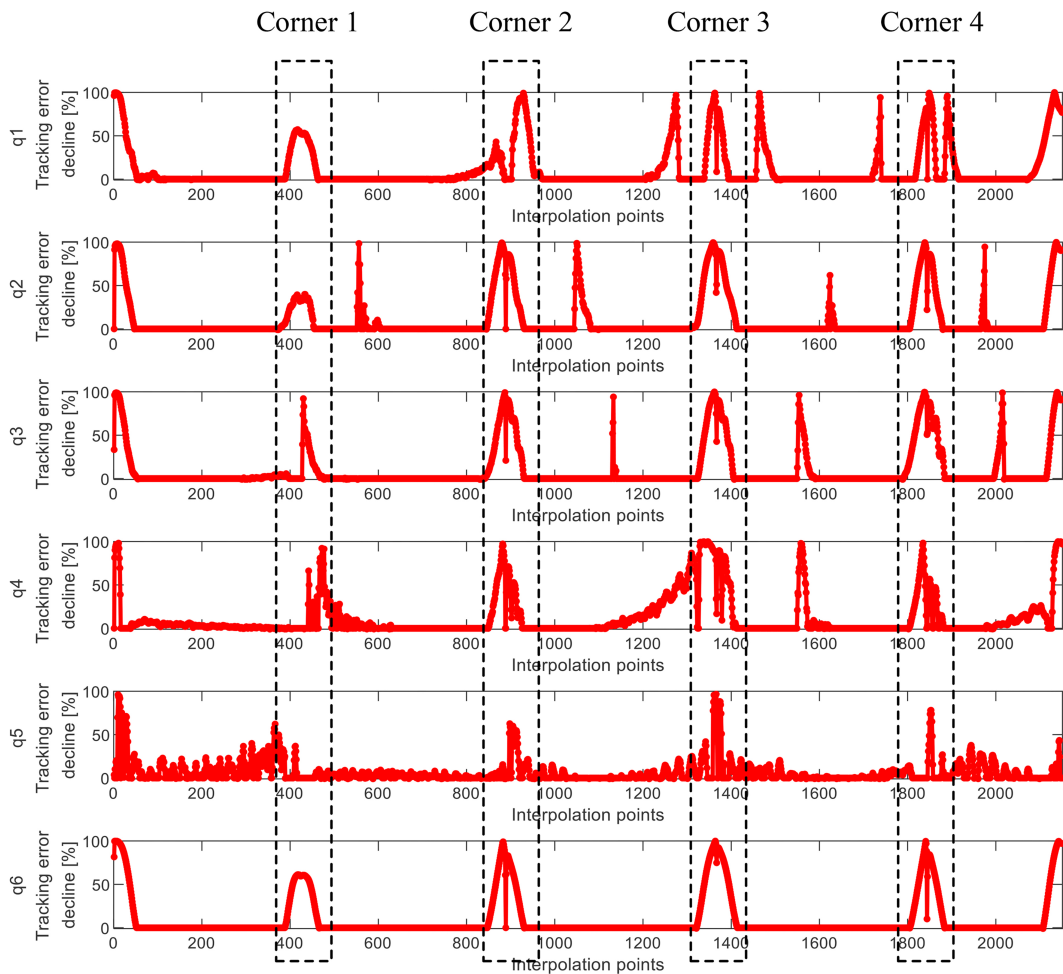


Figure 14. Decrease in the tracking error of each joint position.

## 5. Conclusion

This study proposes a high-performance  $C^3$  continuous tool path smoothing method for a 6R robot manipulator. The proposed method comprehensively considered shape-preserving, redundant angle, and accurate real-time interpolations, which could improve the accuracy and efficiency of robotic machining. To guarantee shape-preserving interpolation after smoothing, the tooltip position and tool orientation are smoothed by the micro spline in the WCS under error tolerance. This study fully utilised the advantages of the PH spline and B-spline. The micro spline replacing the tooltip position corner adopted the  $C^3$  continuous PH spline, which has an analytical arc length and can realise real-time smoothing and interpolation. The tool orientation and redundant angle used the  $C^3$  continuous B-spline, which has a simpler expression than the  $C^3$  continuous PH spline and can further improve the interpolation efficiency. Both the tool orientation and redundant angle are synchronised with the tooltip position by the proposed transitive synchronisation strategy, which is analytical and needs no iteration. Finally, the proposed method obtained jerk continuous joint commands when the redundant angle varies. Compared with the existing corner smoothing algorithm without considering the redundant angle in the simulations, the proposed method realised jerk continuous joint commands and significantly reduced the tracking error.

Because of the use of commercial robots in this experiment, the shortest interpolation cycle is 4 ms. The method proposed in this study can achieve real-time smoothing and interpolation of 0.5 ms. Thus, the method proposed in this study is of great significance for improving the design and manufacture of robots and the machining accuracy of robots.

## Acknowledgements

This research is supported by the National Natural Science Foundation of China (NSFC) under Grant No. 52105528.

## References

- [1] W. Ji and L. Wang, Industrial robotic machining: A review, *International Journal of Advanced Manufacturing Technology*, 103(1–4), 2019, 1239–1255.
- [2] X. Zeng, G. Zhu, Z. Gao, R. Ji, J. Ansari, and C. Lu, Surface polishing by industrial robots: A review, *The International Journal of Advanced Manufacturing Technology*, 125(9–10), 2023, 3981–4012.
- [3] S.H. Kim, E. Nam, T.I. Ha, S.H. Hwang, J.H. Lee, S.H. Park, AND B.K. Min, Robotic machining: A review of recent progress, *International Journal of Precision Engineering and Manufacturing*, 20(9), 2019, 1629–1642.
- [4] Y. Yuan, K. Yu, C. Zhang, Q. Chen, and W. Yang, Generation of textured surfaces by vibration-assisted ball-end milling, *Nanomanufacturing and Metrology*, 1(6), 2023, 19.
- [5] J. Zhao, X. Luo, and Y. Li, A novel robot path planning algorithm based on the improved wild horse optimiser with hybrid strategies, *International Journal of Robotics and Automation*, 39(6), 2024, 515–533.
- [6] Y. Sun, J. Jinjie, X. Jinting, C. Mansen, and N. Jinbo, Path, feedrate and trajectory planning for free-form surface machining: A state-of-the-art review, *Chinese Journal of Aeronautics*, 35(8), 2022, 12–29.
- [7] Y. Ding, Y. Wang, and B. Chen, Smooth and proximate time-optimal trajectory planning of robotic manipulators, *Transactions of the Canadian Society for Mechanical Engineering*, 46(2), 2022, 466–476.
- [8] L. Lu, L. Zhang, C. Fan, and H. Wang, High-order joint-smooth trajectory planning method considering tool-orientation constraints and singularity avoidance for robot surface machining, *Journal of Manufacturing Processes*, 80, 2022, 789–804.
- [9] H. Sun, J. Yang, and H. Ding, A novel tool path smoothing algorithm of 6R manipulator considering pose-dependent dynamics by designing asymmetrical fir filters, *Robotics and Computer-Integrated Manufacturing*, 86, 2024, 102681.
- [10] Z. He, X. Tang, Q. Shen, C. Duan, and C. Jia, Optimisation of a six-degree-of-freedom robot trajectory based on improved multi-objective pso algorithm, *International Journal of Robotics and Automation*, 38(3), 2023, 218–230.
- [11] Y.A. Liu, M. Wan, X.B. Qin, Q.B. Xiao, and W.H. Zhang, Fir filter-based continuous interpolation of g01 commands with bounded axial and tangential kinematics in industrial five-axis machine tools, *International Journal of Mechanical Sciences*, 169(0), 2020, 105325.
- [12] L. Hua, Y. Zhao, J. Zhou, Y. Zhang, N. Huang, and L. Zhu, Five-axis toolpath interpolation method with kinematic corner smoothing and time synchronization, *Journal of Manufacturing Processes*, 105, 2023, 338–358.
- [13] C. Li, Y. Chao, S. Chen, J. Li, and Y. Yuan, Time-optimal trajectory generation for industrial robots based on elite mutation sparrow search algorithm, *International Journal of Robotics and Automation*, 38(2), 2023, 126–135.
- [14] L. Hua, N. Huang, B. Yi, Y. Zhao, and L. Zhu, Global toolpath smoothing for CNC machining based on B-spline approximation with tool tip position adjustment, *The International Journal of Advanced Manufacturing Technology*, 125(7–8), 2023, 3651–3665.
- [15] Q. Xiao, M. Wan, X.B. Qin, Y. Liu, and W.H. Zhang, Real-time smoothing of G01 commands for five-axis machining by constructing an entire spline with the bounded smoothing error, *Mechanism and Machine Theory*, 161, 2021, 104307.
- [16] Q. Xiao, M. Wan, Y. Liu, X.B. Qin, and W.H. Zhang, Space corner smoothing of CNC machine tools through developing 3D general clothoid, *Robotics and Computer-Integrated Manufacturing*, 64, 2020, 101949.
- [17] H. Sun, J. Yang, D. Li, and H. Ding, An on-line tool path smoothing algorithm for 6R robot manipulator with geometric and dynamic constraints, *Science China Technological Sciences*, 64(9), 2021, 1907–1919.
- [18] J. Peng, P. Huang, Y. Ding, and H. Ding, An analytical method for decoupled local smoothing of linear paths in industrial robots, *Robotics and Computer-Integrated Manufacturing*, 72, 2021, 102193.
- [19] H. Xie, Q. Wang, S.K. Ong, A.Y.C. Nee, X. Zhou, and Z. Liao, Automatic generation of interference-free and posture-smooth toolpath for robotic belt grinding of complex workpieces, *IEEE/ASME Transactions On Mechatronics*, 28(1), 2023, 518–530.
- [20] J. Peng, Y. Ding, G. Zhang, and H. Ding, Smoothness-oriented path optimization for robotic milling processes, *Science China Technological Sciences*, 63(9), 2020, 1751–1763.
- [21] N. Huang, L. Hua, X. Huang, Y. Zhang, L. Zhu, and D. Biermann, B-spline-based corner smoothing method to decrease the maximum curvature of the transition curve, *Journal of Manufacturing Science and Engineering, Transactions of the ASME*, 144(5), 2022, 054503.
- [22] X. Liu, Y. Xu, J. Cao, J. Liu, and Y. Zhao, A high-precision planar NURBS interpolation system based on segmentation method for industrial robot, *Applied Sciences*, 13(24), 2023, 13210.
- [23] W. Ma, T. Hu, C. Zhang, and T. Zhang, A robot motion position and posture control method for freeform surface laser treatment based on NURBS interpolation, *Robotics and Computer-Integrated Manufacturing*, 83, 2023, 102547.
- [24] B. Sencer and E. Shamoto, Curvature-continuous sharp corner smoothing scheme for cartesian motion systems, in *Proceeding*

- [25] B. Sencer, K. Ishizaki, and E. Shamoto, A curvature optimal sharp corner smoothing algorithm for high-speed feed motion generation of nc systems along linear tool paths, *The International Journal of Advanced Manufacturing Technology*, 76(9–12), 2015, 1977–1992.
- [26] J. Yang, Q. Qi, A. Adili, and H. Ding, An analytical tool path smoothing algorithm for robotic machining with the consideration of redundant kinematics, *Robotics and Computer-Integrated Manufacturing*, 89, 2024, 102768.
- [27] M. Wan, X.B. Qin, Q.B. Xiao, Y. Liu, and W.H. Zhang, Asymmetrical Pythagorean-hodograph (PH) spline-based C3 continuous corner smoothing algorithm for five-axis tool paths with short segments, *Journal of Manufacturing Processes*, 64, 2021, 1387–1411
- [28] Q. Hu, Y. Chen, X. Jin, and J. Yang, A real-time C3 continuous local corner smoothing and interpolation algorithm for CNC machine tools, *Journal of Manufacturing Science and Engineering-Transactions of the Asme*, 141(4), 2019, 41004.
- [29] R.T. Farouki, J. Manjunathaiah, and G. Yuan, G codes for the specification of Pythagorean-hodograph tool paths and associated feedrate functions on open-architecture CNC machines, *International Journal of Machine Tools & Manufacture*, 39(1), 1999, 123–142.
- [30] D.J. Walton and D.S. Meek, G 2 blends of linear segments with cubics and Pythagorean-hodograph quintics, *International Journal of Computer Mathematics*, 86(9), 2009, 1498–1511.
- [31] R.T. Farouki, C. Giannelli, and A. Sestini, New developments in theory, algorithms, and applications for Pythagorean-hodograph curves, *Springer INdAM Series*, 35, 2019, 127–177.
- [32] R. Ait-Haddou and M. Mazure, Sparse Pythagorean-hodograph curves, *Computer Aided Geometric Design*, 55, 2017, 84–103.
- [33] Q. Hu, Y. Chen, X. Jin, and J. Yang, A real-time C3 continuous tool path smoothing and interpolation algorithm for five-axis machine tools, *Journal of Manufacturing Science and Engineering*, 142(4), 2020, 1–43.
- [34] K. Wu, J. Li, H. Zhao, and Y. Zhong, Review of industrial robot stiffness identification and modelling, *Applied Sciences*, 12(17), 2022, 8719.
- [35] L. Xu, W. Mao, L. Zhu, J. Xu, and Y. Sun, Tool orientation and redundancy integrated planning method constrained by stiffness for robotic machining of freeform surfaces, *The International Journal of Advanced Manufacturing Technology*, 121(11–12), 2022, 8313–8327.
- [36] Y. Ma, Y. Fu, Y. Tian, and X. Liu, Semi-analytical stiffness model of bolted joints in machine tools considering the coupling effect, *Nanomanufacturing and Metrology*, 6(1), 2023, 17.
- [37] X. Zhang, H. Wang, Y. Rong, J. Niu, J. Tian, and Y. Ning, Kinematics and stiffness analysis of a novel 4-DOF over-constrained parallel mechanism with three legs, *International Journal of Robotics and Automation*, 38(6), 2023, 450–460.
- [38] N. Yan, G. Chen, J. Wu, and G. Jin, Trajectory tracking and compensation control of redundant manipulator based on integrated controller, *International Journal of Robotics and Automation*, 37(4), 2022, 362–371.
- [39] S. Zhao, Z. Zhu, C. Chen, Y. Du, X. Song, K. Yan, D. Jiang, L. Li, and A. Liu, Trajectory planning of redundant space manipulators for multi-tasks, *International Journal of Robotics and Automation*, 38(5), 2023, 344–351.
- [40] S. Tulsyan, Local toolpath smoothing for five-axis machine tools, *International Journal of Machine Tools and Manufacture: Design, Research and Application*, 96, 2015, 15–26.

## Biographies



*Qin Hu* was born in Hubei, China, in 1985. She received the M.E. degree in control science and engineering from the Wuhan University of Technology, Hubei, China, in 2011, and the Ph.D. degree in mechanical and electronic engineering from the Huazhong University of Science and Technology, Hubei, China, in 2019. Then, she worked as a Control Engineer for four years. Afterwards, two years of joint training with the University of British Columbia, Canada, between 2017 and 2019. She joined Wuhan University of Technology in 2019, where she is currently an Associate Professor with the School of Automation. Her current research interests include robotic intelligent manufacturing and measurement.



*Runqi Yang* received the B.E. degree in electrical engineering and automation from Shanghai Institute of Technology, China, in 2024. He is currently pursuing the master's degree majoring in control engineering with the Wuhan University of Technology, Hubei, China. He focusses on the field of robot trajectory planning and control. His research mainly revolves around developing efficient and adaptive trajectory planning algorithms for industrial robots. He particularly committed to the design of human-robot interaction control in different environments and the reinforcement learning of robot interaction control, aiming to enhance the navigation ability of robots in complex environments. His work involves a large number of simulations and experimental validations to ensure the robustness and reliability of the proposed algorithms.



*Xu Zhang* is currently pursuing the master's degree in control engineering with the Wuhan University of Technology, Hubei, China. He dedicated to research on robot trajectory planning and 3D measurement. With a strong foundation in robotics and automation, he has acquired extensive knowledge in robotic kinematics, dynamics, and control algorithms. His research focusses on optimising trajectory

planning for industrial robots to improve motion smoothness, reduce energy consumption, and ensure operational safety. Additionally, he is involved in research on point cloud matching and measurement techniques, aiming to enhance 3-D perception and localisation capabilities for robots and autonomous systems. He is proficient in various trajectory planning techniques, including polynomial interpolation and space-based path planning. He aspires to contribute to the advancement of robotic technology and its applications in industrial settings.



*Liang Huang* was born in Hubei, China, in 1979. He received the Ph.D. degree in control science and engineering in 2009. He is currently an Associate Professor with the School of Automation, Wuhan University of Technology, Hubei, China. His primary focus is on artificial intelligence service robots, digital twin 3-D virtual-real interactive control systems, and modular reconfigurable flexible

production systems. His research aims to enhance the intelligence and adaptability of robotic systems through the integration of AI and digital twin technologies. He has published numerous papers in leading journals and conferences, showcasing his innovative contributions to the advancement of intelligent manufacturing and automation. He has successfully led several research projects funded by prestigious grants and has collaborated with many industry players.